NASA

Technical Memorandum TM 79693

Computation of Infrared Cooling Rates in the Water Vapor Bands

Ming-Dah Chou and Albert Arking

NOVEMBER 1978

National Aeronautics and
Space Administration

Goddard Space Flight Center
Greenbelt, Maryland 20771

COMPUTATION OF INFRARED COOLING RATES IN THE WATER VAPOR BANDS

ABSTRACT

A fast but accurate method for calculating the infrared radiative terms due to water vapor has been developed. It makes use of the far wing approximation to scale transmission along an inhomogeneous path to an equivalent homogeneous path. Rather than using standard conditions for scaling, the reference temperatures and pressures are chosen in this study to correspond to the regions where cooling is most significant. This greatly increased the accuracy of the new method. Compared to line by line calculations, the new method has errors up to 4% of the maximum cooling rate, while a commonly used method based upon the Goody band model (Rodgers and Walshaw, 1966) introduces errors up to 11%. The effect of temperature dependence of transmittance has also been evaluated; the cooling rate errors range up to 11% when the temperature dependence is ignored. In addition to being more accurate, the new method is much faster than those based upon the Goody band model.

CONTENTS

TABLES

ILLUSTRATIONS

ILLUSTRATIONS

COMPUTATION OF INFRARED COOLING RATES IN THE WATER VAPOR BANDS

1. Introduction

Absorption, emission, and transmission of thermal infrared radiation by water vapor have a very strong effect on the exchange of radiation energy between atmospheric layers and on the loss of radiation energy to space. Because of the influence of these radiative processes on the thermodynamic structure of the atmosphere, it is important both for modelling the general circulation and for climate modelling to accurately compute the terms involved.

The most accurate methods for computing the radiative terms in a molecular atmosphere involve a detailed "line by line" calculation of the absorption coefficient versus wave number. In recent years, a fairly complete set of line parameters for the important atmospheric gases has been compiled and made available by McClatchey et al. (1973). Although the underlying physics is well understood, the accurate line by line calculation of the radiative terms is a tedious, time consuming process which, for an atmospheric model, must be repeated at each grid point, every time step. Because of computing time limitations these methods are quite impractical for general circulation and climate models. Therefore, the band model and the emissivity method which can avoid the line by line detail are commonly used. For example, GISS GCM (Somerville et al., 1974) partly makes use of the Goody band model to calculate transmittances, and NCAR GCM uses Elssaser and Culbertson's (1960) absorptivity approach with transmittances computed at a fixed temperature (Sasamori, 1968). The diffuse approximation is used to compute diffuse transmittances for both approaches.

In this study we develop a new method for calculating the radiative terms involving water vapor – specifically, the atmospheric cooling rates – which is both fast and accurate. The approach is based upon (1) the actual distribution of line strength and spacing as derived from the line parameter data; and (2) a scaling approximation based upon the behavior in the far wings of absorption lines, which dominate the spectrum. For application to cooling rate calculations in atmospheric models, the method can be made extremely fast by using precomputed tables.

The far wing approximation is developed in Sec. 2. Combined with the k-distribution method, it is applied in Sec. 3 to derive expressions for fluxes and cooling rates. In Sec. 4 we compare cooling rate calculations based upon the new method, the Rodgers and Walshaw method, and the line by line method – the last assumed to be the standard; we also test the validity of other approximations. Concluding remarks appear in Sec. 5.

2. The far-wing approximation

The computation of radiative fluxes and the atmospheric cooling rates involves the calculation of absorption due to thousands of molecular lines. The parameters that determine the absorption coefficient at any wave number ν are the strength, S, half width, α, position ν_o, and shape for each line in the spectrum. The dependence of line strength on temperature varies with each line, while the half width usually has a fixed relationship with temperature and pressure. In computing fluxes over an inhomogeneous path, both line strength and line width change along the path, and these effects must be taken into consideration.

In the troposphere and lower stratosphere, the broadening of lines is primarily due to molecular collisions and therefore the line shape is adequately represented by the Lorentz function. In that case, the absorption coefficient at wave number ν, pressure p, and temperature T is given by

$$k_\nu(p,T) = \sum_i \frac{S_i(T)}{\pi} \frac{\alpha_i(p,T)}{(\nu - \nu_{oi})^2 + \alpha_i^2(p,T)}, \qquad (1)$$

where the summation is over all absorption lines, denoted by the subscript i, the half width is given by $\alpha(p,T) = \alpha(p_r,T_r)\left(\frac{p}{p_r}\right)\left(\frac{T_r}{T}\right)^{1/2}$, and the subscript r denotes reference values.

For any one line, the absorption coefficient increases with decreasing pressure for $|\nu - \nu_o| < \alpha$ and decreases for $|\nu - \nu_o| > \alpha$. In particular, it is proportional to pressure, p, in the far wing of a line and to 1/p at the line center. For atmospheric conditions, the half widths of the absorption lines are small compared to the mean line spacing and, therefore, the wings dominate the spectrum. Furthermore, at those atmospheric levels where water vapor cooling is significant, absorption quickly saturates near the centers of most of the water vapor lines; therefore, errors in the absorption coefficient in the vicinity of line centers will have a small effect on transmittance. These arguments suggest that one might

approximate the pressure and temperature dependence of the absorption coefficient by its behavior in the wings of the lines. At one extreme, where $|\nu - \nu_{oi}| \gg \alpha_i$, the absorption coefficient can be written as

$$k_\nu(p, T) = k_\nu(p_r, T_r) \frac{p}{p_r} R_\nu(T, T_r) , \tag{2}$$

where

$$R_\nu(T, T_r) = \left(\frac{T_r}{T}\right)^{1/2} \frac{\sum_i \left[\frac{S_i(T)\, \alpha_i(p_r, T_r)}{(\nu - \nu_{oi})^2}\right]}{\sum_i \left[\frac{S_i(T_r)\, \alpha_i(p_r, T_r)}{(\nu - \nu_{oi})^2}\right]} . \tag{3}$$

Figs. 1a and b show curves of $R_\nu(T, T_r)$ for specified values of T_r and $T = T_r \pm 40$ K. It can be seen that the absorption coefficient is less sensitive to temperature in the band center region (10-340 cm^{-1}) than in the band wing region (340-580 cm^{-1}). Although the variation of $R_\nu(T, T_r)$ with wave number is large, it is still small compared to the variation of k_ν. If we replace $R_\nu(T, T_r)$ by its mean value, $\bar{R}(T, T_r)$, over a wide spectral interval, Eq. (2) becomes

$$k_\nu(p, T) = k_\nu(p_r, T_r) \frac{p}{p_r} \bar{R}(T, T_r) . \tag{4}$$

The use of (4) to represent the temperature and pressure dependence of $k_\nu(p, T)$ will be called the "far wing approximation." The advantage of this approximation is the separation of ν from the variables p and T. As will be seen later, it leads to a great simplification in the computation of the radiative terms.

The errors introduced by the far-wing approximation will not be large because of the rapid decrease of water vapor mixing ratio with height. This causes the vertical profile of cooling rate due to any spectral region to have a sharp peak, thus spanning relatively narrow ranges of temperature and pressure. Within those narrow ranges, Eq. (4) would be expected to be fairly accurate.

The reference parameters p_r and T_r could be fixed for the entire water vapor spectrum or one can divide the spectrum into several regions, with p_r and T_r chosen in each region to correspond to conditions at the level of maximum influence on cooling rates. We found that one can obtain very good accuracy by dividing the water vapor spectrum (including both the 6.3 μm and the rotational bands) into only two *types* of spectral regions: (1) the vicinity of the *band centers*, where absorption is strong; and (2) the *band wings*, where absorption is moderate. The assignment of spectral regions to band wings and band centers is shown in Table 1. The reference parameters were chosen to be p_r = 275 mb, T_r = 225 K for the band centers and p_r = 550 mb, T_r = 256 K for the band wings; they correspond to points on the temperature versus pressure curve for a mid-latitude standard atmosphere (see Fig. 2a), where each spectral region type contributes most significantly to the cooling rate. Also tabulated in Table 1 are the values $\bar{R}$ at $T_r \pm 40$ K for the two band regions. As is well known, the table shows that the band wings are much more sensitive to temperature than the band centers. Rather than calculate $\bar{R}(T, T_r)$ at a large number of temperatures, we took advantage of its expected smooth behavior and used a polynomial fit to the values at $T = T_r - 40$, $T = T_r$ (for which $\bar{R} = 1$) and $T = T_r + 40$.

The computational advantage of the far wing approximation will become obvious in the next section when calculating the transmittance through an atmospheric layer averaged over a wide spectral interval. Meanwhile, the monochromatic transmittance between pressure levels p_1 and p_2, for radiation in a direction forming the angle $\cos^{-1}\mu$ with respect to the zenith axis, is given by

$$\tau\left(u_\nu(p_1, p_2)\right) = e^{-\frac{1}{\mu} u_\nu(p_1, p_2)} \tag{5}$$

where $u_\nu(p_1, p_2)$ is the optical thickness of the layer, defined by

$$u_\nu(p_1, p_2) = \int_{p_1}^{p_2} \frac{1}{g} k_\nu(p, T(p))\, q(p)\, dp, \tag{6}$$

q is the specific humidity and g is the gravitational acceleration.

In the far wing approximation, the optical thickness becomes

$$u_\nu(p_1, p_2) = k_\nu(p_r, T_r)\, \bar{w}(p_1, p_2) \tag{7}$$

where

$$\bar{w}(p_1, p_2) = \int_{p_1}^{p_2} \frac{1}{g} \frac{p}{p_r} \bar{R}\left(T(p), T_r\right) q(p)\, dp \tag{8}$$

is the amount of water vapor in the layer, scaled by the factor $(p/p_r)\,\bar{R}\left(T(p), T_r\right)$. The scaling factor is a function not only of the ambient temperature and pressure but also of the selected reference conditions, p_r and T_r. This constitutes a one-parameter scaling approximation. It differs in a rather significant way from the more commonly used scaled water vapor amount (Elsasser and Culbertson, 1960; Manabe and Möller, 1961; Lacis and Hansen, 1974; Ramanathan, 1976; Wang, 1976)

$$\bar{w}'(p_1, p_2) = \int_{p_1}^{p_2} \frac{1}{g} \left(\frac{p}{p_r}\right)^m \left[\frac{T_r}{T(p)}\right]^n q(p)\, dp, \tag{9}$$

where $0 < m \leq 1$ and $n \geq 0$. Eq. (9) implies that absorption decreases with increasing temperature, quite the contrary of what actually happens, as revealed in Fig. 1 and Table 1. Of the two factors in (3) which determine the temperature dependence of the absorption coefficient, the second one is effectively ignored by the use of (9), and that turns out to be the dominant factor. Another important difference between $\bar{w}(p_1, p_2)$ and $\bar{w}'(p_1, p_2)$ is the choice of reference levels: in utilizing $\bar{w}'(p_1, p_2)$, the reference conditions were always chosen at 1 atmosphere, thus introducing a large error in the middle and upper troposphere, where cooling due to water vapor is large (as will be seen below). By judicious choice of reference values, the error is significantly reduced at the important levels.

To test the accuracy of the far wing approximation, transmittances were calculated monochromatically at .01 cm^{-1} intervals for $\mu = 1$ between typical atmospheric levels for the mid-latitude atmosphere shown in Figs. 2a and 2b. Fig. 3 shows the transmittances between 100 and 250 mb (Fig. 3a) and between 250 and 400 mb (Fig. 3b) plotted against wave number in the range 320 to 340 cm^{-1} (near band center), and Fig. 4 shows transmittance between 300 and 600 mb for wave numbers 460 to 480 cm^{-1} (band wing region). In each graph, the solid curve is an "exact" calculation based upon the Voigt profile, taking into account its pressure and temperature variation along the path. The dashed curve represents the "far wing approximation," in which the absorption coefficient is computed according to (4). As might be expected, the far wing approximation is better for those layers close to the reference conditions.

Mean transmittance over 20 cm^{-1} wave number intervals for various atmospheric layers is shown in Table 2. It is seen that even far from the reference conditions the error is $\lesssim .01$. Over wider spectral intervals the errors are smaller.

3. Fluxes and cooling rates

In a non-scattering atmosphere with temperature profile T(p), the monochromatic upward and downward fluxes of thermal radiation due to water vapor at pressure level p are given by

$$F_\nu^{\uparrow}(p) = B_\nu(T_s)\ \hat{\tau}\ \left(u_\nu(p, p_s)\right) - \int_p^{p_s} B_\nu\left(T(p')\right)\ \frac{d\hat{\tau}(u_\nu(p, p'))}{dp'}\ dp' \qquad (10a)$$

$$F_\nu^{\downarrow}(p) = \int_0^{p} B_\nu\left(T(p')\right)\ \frac{d\hat{\tau}(u_\nu(p, p'))}{dp'}\ dp' \qquad (10b)$$

where $B_\nu(T)$ is the Planck flux (i.e., π times the usual Planck function), $u_\nu(p, p')$ is the optical thickness defined by (6), and $\hat{\tau}(u)$ is the diffuse transmittance, which is proportional to the third exponential integral,

$$\hat{\tau}(u) = 2E_3(u), \qquad (11)$$

$$E_n(u) = \int_1^{\infty} \frac{e^{-ut}}{t^n}\ dt\ ,$$

In (10), p_s denotes surface pressure, and T_s denotes temperature of the surface itself, which could differ from the air temperature immediately above the surface, $T(p_s)$.

The cooling rate at any level is related to the divergence of the net flux at that level integrated over wave number,

$$-\frac{\partial T(p)}{\partial t} = -\frac{g}{C_p}\frac{d}{dp}\int\left[F_\nu^{\uparrow}(p) - F_\nu^{\downarrow}(p)\right] d\nu\ , \qquad (12)$$

where C_p is the specific heat of air at constant pressure and t is time. In the numerical examples considered here, the integration over wave number is carried out only for the portions of the water vapor spectrum listed in Table 1.

For computational convenience, we integrate (10a) and (10b) by parts and subtract one from the other to obtain

$$F_\nu^{\uparrow}(p) - F_\nu^{\downarrow}(p) = \left[B_\nu(T_s) - B_\nu\left(T(p_s)\right)\right] \hat{\tau}\left(u_\nu(p, p_s)\right) + B_\nu\left(T(0)\right) \hat{\tau}\left(u_\nu(0,p)\right) + \int_{T(0)}^{T(p)} \hat{\tau}\left(u_\nu(p',p)\right) \left.\frac{dB_\nu(T)}{dT}\right|_{T(p')} dT(p') + \int_{T(p)}^{T(p_s)} \hat{\tau}\left(u_\nu(p,p')\right) \left.\frac{dB_\nu(T)}{dT}\right|_{T(p')} dT(p') \tag{13}$$

where T(0) represents the temperature at the top of the atmosphere ($p \approx 0$).

Making use of the far wing approximation, as embodied in (7), and defining the function

$$G(\bar{w}, T) = \int \hat{\tau}\left(\bar{w} k_\nu(p_r, T_r)\right) B_\nu(T)\, d\nu \ , \tag{14}$$

the cooling rate becomes

$$-\frac{\partial T(p)}{\partial t} = -\frac{g}{C_p}\frac{d}{dp}\left[G\left(\bar{w}(p, p_s), T_s\right) - G\left(\bar{w}(p, p_s), T(p_s)\right) + G\left(\bar{w}(0, p), T(0)\right) + \int_{T(0)}^{T(p)} \frac{\partial G}{\partial T}\left(\bar{w}(p', p), T(p')\right) dT(p') + \int_{T(p)}^{T(p_s)} \frac{\partial G}{\partial T}\left(\bar{w}(p, p'), T(p')\right) dT(p')\right]. \tag{15}$$

The function G can be rapidly computed via the k-distribution method (Arking and Grossman, 1972). We divide the spectrum into n intervals $\Delta\nu_i = \nu_i - \nu_{i-1}$, i = 1, ..., n, and let $B_i(T)$ be a suitable mean of $B_\nu(T)$ in the i^{th} interval. [Here there is an implicit assumption that for each interval $\nu_{i-1} \leq \nu \leq \nu_i$, $|B_i(T) - B_\nu(T)|$ and its derivative are smaller than acceptable upper bounds.] Letting $x = \log k$, x_i^{min} and x_i^{max} the minimum and maximum values of x in the i^{th} interval, and $h_i(x)$ the distribution of $x = \log k(p_r, T_r)$ normalized so that

$$\int_{x_i^{min}}^{x_i^{max}} h_i(x)\, dx = 1,$$

then the mean *diffuse* transmittance in the interval, as a function of the scaled water vapor amount, becomes

$$\hat{\tau}_i(\bar{w}) = 2\int_{x_i^{min}}^{x_i^{max}} E_3(\bar{w}k)\, h_i(x)\, dx \qquad (16)$$

The function G can then be expressed in terms of $\bar{\tau}_i(\bar{w})$ as follows:

$$G(\bar{w}, T) = \sum_{i=1}^{n} B_i(T)\, \hat{\tau}_i(\bar{w})\, \Delta\nu_i \qquad (17)$$

Using the line parameters compiled by McClatchey et al. (1972) and assuming a Voigt line profile, the k-distribution function, h(x), has been computed, and the results are listed in Tables 3 and 4, respectively, for the band center and the band wing regions at selected reference conditions. For repeated rapid computations one can store either the function $\hat{\tau}_i(\bar{w})$ or $G(\bar{w}, T)$ and use it in a table lookup procedure. For the examples considered here, we employed the latter scheme; G is tabulated separately for the band center and band wing regions in Tables 5 and 6, respectively. The function behaves rather smoothly and is capable of providing high accuracy with minimal tabulation.

4. Comparison of methods

a. Testing approximations line by line

As a standard for testing various approximations, transmittances and cooling rates were calculated line by line and averaged over the appropriate spectral intervals. There are many ways of carrying out these calculations: line shapes and functional dependences have to be specified and appropriate numerical schemes must be employed. Nevertheless, the line by line calculations employed here will be treated as "exact" for purposes of comparing the accuracies of various approximations and computational methods. The method for the line by line calculations will be fully described by Arking and Chesters (1979) and briefly described as follows.

The calculations are based upon the line parameters for the H_2O molecule compiled by McClatchey et al. (1972). The line shape is assumed to be a Voigt profile cut off at 10 cm^{-1} from the line center, and the Lorentz half-width is assumed to be proportional to $p/\sqrt{T}$. The atmosphere is assumed to consist of 39 layers overlying a blackbody surface. Each layer is treated as if it were isothermal at a temperature corresponding to the arithmetic mean of the temperatures at the upper and lower boundaries of the layer. The surface is assumed to be at 1000 mb and the top of the atmosphere at 0.2 mb. Using an accurate algorithm for the pressure integral of the Voigt function developed by Milman (1976), the integral of the absorption coefficient between each pair of levels is calculated monochromatically at intervals of .01 cm^{-1} These integrals constitute the optical thickness between levels defined by (6). Monochromatic transmitance is then given by (5) and the cooling rates by (10) and (12).

The cooling rates were calculated line by line exactly as just described and with three different approximations: (1) the *far wing approximation*, where Eq. (4) is used; (2) the *isothermal approximation*, where the absorption coefficient is computed at 250 K but pressure dependence is taken into account exactly; and (3) the *diffusivity approximation*, where the diffuse transmittance, $2\,E_3(u)$, is replaced by $\exp(-1.66\,u)$.

Fig. 5a shows the exact cooling rates for the 200-580 cm^{-1} region. The lower wave numbers are near the center of the water vapor rotational band, and the higher wave numbers are in the wing of the band. It can be seen that the level of maximum cooling rate shifts upward as absorption increases. The differences between the exact cooling rate and that computed using the three approximations are shown in Fig. 5b (approximation minus exact). It can be seen that the far-wing approximation introduces only small errors with a maximum magnitude less than 2% of the peak cooling rate. It is comparable to the error associated with the commonly used diffusivity approximation. In the 200-580 cm^{-1} spectral region, the mean intensity transmittance, τ, decreases with increasing water vapor amount, w, nearly according to the strong line approximation

$$\tau(cw) \cong \exp[-(cw)^{1/2}],$$

and the mean diffuse transmittance, $\hat{\tau}$, is approximately given by

$$\hat{\tau}(cw) \cong 2\int_0^1 \exp[-(cw/\mu)^{1/2}\mu\, d\mu] = 4E_5[(cw)^{1/2}],$$

where c is a function of temperature, pressure, and spectral interval. It is found that the difference between $\exp[-(1.66\ cw)^{1/2}]$ and $4E_5[(cw)^{1/2}]$ is less than 0.01 for all values of cw. Therefore, the use of the diffusivity approximation which amplifies the water vapor amount by a factor of 1.66 for the diffuse transmittance computations induces only small errors in the computed cooling rates.

For the isothermal approximation, the emission is correctly computed near the 400-mb level where the temperature is equal to 250 K for the tropical profile used. Since the tropospheric temperature decreases with increasing height, and since absorption decreases with decreasing temperature, the atmosphere is computed too transparent below and too opaque above

the 400-mb level. Accordingly, both the computed incoming upward and downward fluxes at the 400-mb level are larger than the exact ones, and more energy is absorbed near the 400-mb level. The effect of over-estimating the energy absorbed near 400 mb reduces the cooling rate, as seen in Fig. 5b. The maximum error is 11% of the peak cooling rate.

b. Present method compared with the Rodgers-Walshaw method

The cooling rate calculations of Rodgers and Walshaw (1966) are based upon Goody's statistical band model for water vapor transmittance. The inhomogeneity of the atmosphere is taken into account by using the Curtis-Godson approximation, the diffusivity approximation is used for computing diffuse transmittances, and the spectrum is divided into a number of intervals, depending upon the desired accuracy. In this study we used 34 intervals, of 40 cm^{-1} each. (For application to atmospheric models, such as in the GISS GCM, the use of such fine intervals is considered too time consuming; instead, the intervals are 200 cm^{-1}.)

In the present method there is no need for a large number of intervals. Instead, each portion of the spectrum is assigned to either of two region types, *band centers* or *band wings* and the spectral regions of each type are combined. The function $G(\bar{w}, T)$ defined by (14) is pre-computed for each region type and the cooling rates are computed from (15).

In order to compare the Rodgers-Walshaw method with the present method, the cooling rate is computed exactly for the tropical and sub-arctic model atmospheres and is shown in Fig. 6a. It can be seen that the major contribution of the water vapor bands is in the mid-troposphere with a maximum near the 300-mb level for the tropical model and 550 mb for the sub-arctic winter model. Near the surface and in the upper troposphere and above, the atmosphere is either too opaque or too transparent to have significant cooling.

The errors (measured against the line by line calculations) in the cooling rate computed from the present method and the Rodgers-Walshaw method are shown in Figs. 6b and 6c for the tropical and sub-arctic winter cases, respectively. The cooling rate error of the present

method is very small with a maximum magnitude of 4% of the peak cooling rate, while the maximum error of the Rodgers-Walshaw method is 11% of the peak cooling rate.

The upward fluxes at the top of the atmosphere, $F\uparrow(0)$, and the downward fluxes at the earth's surface, $F\downarrow(p_s)$, for the tropical and sub-arctic winter atmospheres are shown in Table 7. It can be seen that in both the present method and the Rodgers-Walshaw method the errors are small. Because of the use of (4) in the present method, transmittances are computed too large in the upper troposphere and too small near the surface, and consequently the effective emitting levels for $F\uparrow(0)$ and $F\downarrow(p_s)$ are shifted downward. Therefore, both $F\uparrow(0)$ and $F\downarrow(p_s)$ are larger than the exact ones. For the Rodgers-Walshaw method, the computed transmittances are generally too small, and hence the value of $F\uparrow(0)$ is too small and that of $F\downarrow(p_s)$ is too large compared to the exact ones.

c. The effect of the e-type continuous absorption

The results shown in this study were obtained by including only the absorption by water vapor lines; e-type continuous absorption was not considered. We have investigated the effect of e-type absorption in the 400-580 cm^{-1} spectral region for the tropical model atmosphere. Using the line by line calculation, it has been found that the effect is to reduce the transmittance and, hence, the cooling rate by 0.15° C/day in the 900-1000 mb region. Above the 900-mb level, the effect is very small. For drier atmospheres, the effect of the e-type absorption in the water vapor bands can be neglected. In another study (Chow and Arking, 1978), e-type continuum absorption and the 10 μm window region were included in the computation of cooling rates.

5. Summary and further remarks

An accurate but fast method has been developed for infrared flux computations in the water vapor bands. The absorption coefficient at any part of the atmosphere is computed from the absorption coefficient at the reference conditions using the far-wing approximation for which the dependence of the absorption coefficient on pressure and temperature is assumed to correspond to that of the wings of absorption lines. The present method differs from the commonly used one-parameter scaling by suitably choosing the reference conditions corresponding to the regions where cooling is most significant. With the use of the far-wing approximation, the wavenumber dependence of the absorption coefficient can be separated from pressure and temperature, and the computation is greatly simplified. Further reduction of the computation is achieved by dividing the entire water vapor spectrum into only two regions (band center and wing regions) and using the pre-computed tables.

Using the exact line-by-line calculation as a standard, the accuracy of the present method is compared with that of Rodgers and Walshaw. It has been found that the present method introduces a maximum error of only 4% of the peak cooling rate, while the Rodgers-Walshaw method introduces an 11% error. The upward fluxes at the top of the atmosphere and the downward fluxes at the earth's surface were also compared with the exact line-by-line calculations; the errors in these fluxes are small with a magnitude less than 2% for both the present method and the Rodgers-Walshaw method.

The accuracy of the far-wing approximation was also compared with the commonly used diffusivity and isothermal approximations. For the diffusivity approximation, the diffuse transmittance was computed as the intensity transmittance but the optical thickness was amplified by a factor of 1.66. For the isothermal approximation, the transmittance was computed at a temperature of 250 K. It has been found that both the far-wing and the diffusivity approximations introduce only small errors in the computed cooling rates with

a maximum error $\lesssim 2\%$ of the peak cooling rate, while the isothermal approximation introduces large errors ($\sim 11\%$). The cooling rate for the isothermal approximation is underestimated in the neighborhood of the 250 K level and is overestimated near the surface and in the upper troposphere.

REFERENCES

Arking, A., and D. Chesters, 1979: An efficient line by line method for calculating atmospheric transmittance, in preparation.

Arking, A., and K. Grossman, 1972: The influence of line shape and band structure on temperatures in planetary atmospheres. *J. Atmos. Sci.*, 29, 937-949.

Chow, M.-D., and A. Arking, 1977: An infrared radiation routine for use in numerical atmospheric models. Preprints, Third Conference on Atmospheric Radiation, Amer. Meteor. Society, 303–305.

Elsasser, W. M. and M. F. Culbertson, 1960: Atmospheric radiation tables. *Meteor. Monogr.*, 4, No. 23, 43 pp.

Lacis, A. A., and J. E. Hansen, 1974: A parameterization for the absorption of solar radiation in the earth's atmosphere. *J. Atmos. Sci.*, 31, 118-133.

Manabe, S., and F. Möller, 1961: On the radiative equilibrium and heat balance of the atmosphere. *Mon. Wea. Rev.*, 89, 503-532.

McClatchey, R. A., R. W. Fenn, J. E. A. Selby, F. E. Volz, and J. S. Garing, 1972: Optical properties of the atmosphere (third edition). *Environ. Res. Pap.*, No. 411, AFCRL-72-0497.

McClatchey, R. A., W. S. Benedict, S. A. Clough, D. E. Burch, R. F. Calfee, K. Fox, L. S. Rothman, and J. S. Garing, 1973: AFCRL atmospheric absorption line parameters compilation. *Environ. Res. Pap.*, No. 434, AFCRL-TR-73-0096.

Milman, A. S., 1976: Evaluation of an integral of the Voigt function. CSC/TM/6183, Computer Sciences Corporation, pp 29.

Ramanathan, V., 1976: Radiative transfer within the earth's troposphere and stratosphere: a simplified radiative-convective model. *J. Atmos. Sci.*, 33, 1330-1346.

Rodgers, C. D., and C. D. Walshaw, 1966: The computation of infra-red cooling rate in planetary atmospheres. *Quart. J. Roy. Meteor. Soc.*, 92, 67-92.

Sasamori, T., 1968: The radiative cooling calculation for application to general circulation experiments. *J. Appl. Meteor.*, 7, 721-729.

Somerville, R. C. J., P. H. Stone, M. Halem, J. E. Hansen, J. S. Hogan, L. M. Druyan, G. Russell, A. A. Lacis, W. J. Quirk, and J. Tenenbaum, 1974: The GISS model of global atmosphere. *J. Atmos. Sci.*, 31, 84-117.

Wang, W.-C., 1976: A parameterization for the absorption of solar radiation by water vapor in the earth's atmosphere. *J. Appl. Meteor.*, 15, 21-27.

Table 1. The reference temperature T_r and pressure p_r are specified for the center and the wing regions of the water vapor absorption bands. The effect of temperature on the absorption coefficient is indicated by $\bar{R}(T, T_r)$, which is the mean value of the function $R_\nu(T, T_r)$ defined by Eq. (3).

	Wave number (cm^{-1})	T_r(K)	p_r(mb)	$\bar{R}(T_r - 40\,K, T_r)$	$\bar{R}(T_r + 40\,K, T_r)$
Center	0-340 1380-1900	225	275	0.90	1.16
Wing	340-580 1220-1380 1900-2020	256	550	0.58	1.78

Table 2. Mean intensity transmittance over 20 cm^{-1} spectral intervals.

320-340 cm^{-1}			460-480 cm^{-1}		
Layer (mb)	"Exact" transmittance	Model transmittance	Layer (mb)	"Exact" transmittance	Model transmittance
10-100	0.910	0.915	10-100	0.987	0.996
100-250	0.814	0.815	100-300	0.951	0.957
250-400	0.350	0.357	300-600	0.530	0.531
400-500	0.116	0.125	600-850	0.162	0.161
500-600	0.025	0.036	850-1000	0.100	0.099

Table 3. The k-distribution function for the band center region with p_r = 275 mb and T_r = 225 K.

Wave number (cm^{-1})	$\log_{10}$ k														
	-1.00	-0.75	-0.50	-0.25	0.0	0.25	0.50	0.75	1.00	1.25	1.50	1.75	2.00	2.25	2.50
20- 60	0.0	0.0	0.0	0.0	0.0	0.0	0.101	0.476	0.263	0.505	0.547	0.301	0.230	0.321	0.333
60- 100	0.0	0.0	0.0	0.0	0.0	0.0	0.0	0.0	0.0	0.0	0.109	0.254	0.513	0.682	0.602
100- 140	0.0	0.0	0.0	0.0	0.0	0.0	0.0	0.0	0.0	0.0	0.253	0.102	0.464	0.815	0.511
140- 180	0.0	0.0	0.0	0.0	0.0	0.0	0.0	0.0	0.0	0.0	0.331	0.414	0.401	0.537	0.512
180- 220	0.0	0.0	0.0	0.0	0.0	0.0	0.0	0.0	0.0	0.097	0.256	0.140	0.149	0.357	0.261
220- 260	0.0	0.0	0.0	0.0	0.0	0.0	0.008	0.379	0.374	0.301	0.223	0.268	0.435	0.501	0.397
260- 300	0.0	0.0	0.0	0.0	0.0	0.0	0.0	0.686	0.707	0.543	0.469	0.239	0.212	0.355	0.227
300- 340	0.0	0.0	0.0	0.0	0.0	0.0	0.300	0.798	0.661	0.430	0.433	0.335	0.221	0.159	0.136
1380-1420	0.0	0.0	0.041	0.288	0.433	0.577	0.585	0.449	0.337	0.339	0.259	0.170	0.127	0.088	0.088
1420-1460	0.0	0.0	0.0	0.0	0.203	0.309	0.427	0.662	0.653	0.385	0.279	0.226	0.227	0.185	0.103
1460-1500	0.0	0.0	0.0	0.0	0.0	0.010	0.339	0.366	0.721	0.607	0.466	0.345	0.324	0.220	0.162
1500-1540	0.0	0.0	0.0	0.0	0.0	0.0	0.0	0.0	0.164	0.432	0.782	0.607	0.355	0.385	0.323
1540-1580	0.0	0.0	0.0	0.0	0.0	0.0	0.0	0.0	0.272	0.722	0.602	0.491	0.420	0.352	0.269
1580-1620	0.0	0.076	0.099	0.155	0.210	0.640	0.449	0.603	0.428	0.331	0.276	0.209	0.138	0.113	0.080
1620-1660	0.0	0.0	0.0	0.0	0.0	0.0	0.0	0.0	0.570	0.767	0.454	0.528	0.386	0.322	0.216
1660-1700	0.0	0.0	0.0	0.0	0.0	0.0	0.0	0.0	0.249	0.680	0.638	0.638	0.448	0.332	0.257
1700-1740	0.0	0.0	0.0	0.0	0.0	0.0	0.178	0.320	0.452	0.538	0.466	0.506	0.356	0.287	0.236
1740-1780	0.0	0.0	0.0	0.0	0.0	0.0	0.162	0.645	0.508	0.759	0.432	0.390	0.290	0.226	0.170
1780-1820	0.0	0.0	0.074	0.362	0.161	0.475	0.475	0.490	0.501	0.385	0.275	0.217	0.167	0.115	0.079
1820-1860	0.114	0.108	0.098	0.319	0.297	0.529	0.527	0.557	0.370	0.264	0.196	0.144	0.147	0.089	0.064
1860-1900	0.086	0.395	0.386	0.679	0.664	0.447	0.279	0.174	0.220	0.160	0.143	0.103	0.070	0.051	0.038

Table 3. (Continued)

Wave number (cm^{-1})	$\log_{10} k$														
	2.75	3.00	3.25	3.50	3.75	4.00	4.25	4.50	4.75	5.00	5.25	5.50	5.75	6.00	6.25
20- 60	0.213	0.191	0.136	0.101	0.083	0.073	0.053	0.030	0.024	0.011	0.008	0.0	0.0	0.0	0.0
60- 100	0.463	0.389	0.303	0.172	0.128	0.119	0.088	0.069	0.043	0.039	0.014	0.008	0.005	0.0	0.0
100- 140	0.372	0.326	0.322	0.220	0.167	0.128	0.107	0.072	0.049	0.035	0.029	0.016	0.012	0.0	0.0
140- 180	0.444	0.351	0.253	0.177	0.176	0.122	0.080	0.059	0.043	0.040	0.024	0.018	0.007	0.006	0.0
180- 220	0.207	0.156	0.097	0.070	0.052	0.035	0.026	0.018	0.026	0.017	0.014	0.013	0.005	0.004	0.0
220- 260	0.267	0.230	0.172	0.125	0.090	0.061	0.043	0.034	0.035	0.023	0.015	0.009	0.007	0.003	0.0
260- 300	0.154	0.105	0.069	0.063	0.042	0.041	0.030	0.024	0.015	0.012	0.004	0.003	0.0	0.0	0.0
300- 340	0.161	0.094	0.063	0.063	0.041	0.027	0.026	0.019	0.020	0.007	0.003	0.003	0.0	0.0	0.0
1380-1420	0.065	0.041	0.035	0.029	0.023	0.014	0.008	0.004	0.0	0.0	0.0	0.0	0.0	0.0	0.0
1420-1460	0.075	0.062	0.066	0.060	0.030	0.026	0.010	0.008	0.004	0.0	0.0	0.0	0.0	0.0	0.0
1460-1500	0.121	0.090	0.065	0.051	0.036	0.032	0.027	0.016	0.002	0.0	0.0	0.0	0.0	0.0	0.0
1500-1540	0.303	0.194	0.139	0.104	0.076	0.055	0.034	0.024	0.017	0.006	0.0	0.0	0.0	0.0	0.0
1540-1580	0.224	0.177	0.121	0.100	0.074	0.063	0.053	0.028	0.020	0.012	0.0	0.0	0.0	0.0	0.0
1580-1620	0.065	0.044	0.031	0.015	0.014	0.006	0.006	0.004	0.004	0.004	0.0	0.0	0.0	0.0	0.0
1620-1660	0.177	0.155	0.125	0.086	0.058	0.052	0.048	0.029	0.015	0.012	0.0	0.0	0.0	0.0	0.0
1660-1700	0.182	0.128	0.128	0.107	0.071	0.048	0.040	0.024	0.016	0.012	0.002	0.0	0.0	0.0	0.0
1700-1740	0.138	0.143	0.101	0.087	0.075	0.039	0.038	0.026	0.012	0.002	0.0	0.0	0.0	0.0	0.0
1740-1780	0.123	0.087	0.072	0.043	0.038	0.021	0.020	0.010	0.004	0.0	0.0	0.0	0.0	0.0	0.0
1780-1820	0.066	0.049	0.038	0.029	0.020	0.012	0.004	0.004	0.002	0.0	0.0	0.0	0.0	0.0	0.0
1820-1860	0.047	0.031	0.040	0.017	0.018	0.014	0.006	0.004	0.0	0.0	0.0	0.0	0.0	0.0	0.0
1860-1900	0.035	0.027	0.015	0.012	0.008	0.006	0.002	0.0	0.0	0.0	0.0	0.0	0.0	0.0	0.0

Table 4. The k-distribution function for the band wing region with p_r = 550 mb and T_r = 256 K.

Wave number (cm^{-1})	$\log_{10}$ k														
	-2.50	-2.25	-2.00	-1.75	-1.50	-1.25	-1.00	-0.75	-0.50	-0.25	0.0	0.25	0.50	0.75	1.00
340- 380	0.0	0.0	0.0	0.0	0.0	0.0	0.0	0.0	0.0	0.0	0.0	0.260	0.299	0.242	0.569
380- 420	0.0	0.0	0.0	0.0	0.0	0.0	0.0	0.070	0.104	0.261	0.335	0.480	0.623	0.399	0.243
420- 460	0.0	0.0	0.0	0.0	0.0	0.0	0.0	0.0	0.0	0.080	0.525	0.672	0.511	0.498	0.498
460- 500	0.0	0.0	0.0	0.0	0.0	0.0	0.0	0.231	0.297	0.815	0.531	0.583	0.477	0.300	0.194
500- 540	0.0	0.0	0.0	0.0	0.0	0.0	0.123	0.380	0.369	0.547	0.472	0.544	0.407	0.324	0.205
540- 580	0.0	0.0	0.0	0.0	0.0	0.115	0.199	0.408	0.856	0.602	0.434	0.403	0.247	0.205	0.154
1220-1260	0.196	0.216	0.120	0.470	0.605	0.609	0.488	0.369	0.280	0.227	0.169	0.112	0.055	0.030	0.018
1260-1300	0.0	0.0	0.0	0.0	0.212	0.476	0.514	0.527	0.454	0.411	0.432	0.276	0.203	0.162	0.111
1300-1340	0.0	0.0	0.0	0.094	0.152	0.121	0.079	0.200	0.368	0.588	0.517	0.326	0.368	0.336	0.212
1340-1380	0.0	0.0	0.0	0.0	0.0	0.0	0.0	0.0	0.070	0.361	0.481	0.473	0.705	0.443	0.332
1900-1940	0.0	0.0	0.0	0.0	0.0	0.0	0.0	0.584	0.242	0.420	0.739	0.417	0.450	0.327	0.220
1940-1980	0.0	0.0	0.0	0.103	0.082	0.116	0.336	0.500	0.562	0.470	0.362	0.289	0.277	0.197	0.205
1980-2020	0.0	0.0	0.0	0.0	0.183	0.438	0.579	0.538	0.507	0.322	0.330	0.288	0.204	0.154	0.107

Table 4. (Continued)

Wave number (cm^{-1})	$\log_{10} k$														
	1.25	1.50	1.75	2.00	2.25	2.50	2.75	3.00	3.25	3.50	3.75	4.00	4.25	4.50	4.75
340- 380	0.496	0.263	0.302	0.444	0.354	0.213	0.137	0.114	0.087	0.073	0.061	0.046	0.023	0.012	0.002
380- 420	0.197	0.204	0.218	0.135	0.216	0.149	0.111	0.083	0.060	0.049	0.034	0.022	0.007	0.0	0.0
420- 460	0.327	0.205	0.190	0.129	0.112	0.080	0.063	0.063	0.028	0.011	0.005	0.003	0.0	0.0	0.0
460- 500	0.142	0.115	0.085	0.051	0.054	0.051	0.033	0.018	0.017	0.006	0.0	0.0	0.0	0.0	0.0
500- 540	0.188	0.130	0.090	0.065	0.044	0.036	0.026	0.029	0.013	0.008	0.0	0.0	0.0	0.0	0.0
540- 580	0.100	0.080	0.060	0.054	0.035	0.030	0.013	0.003	0.002	0.0	0.0	0.0	0.0	0.0	0.0
1220-1260	0.015	0.013	0.008	0.0	0.0	0.0	0.0	0.0	0.0	0.0	0.0	0.0	0.0	0.0	0.0
1260-1300	0.084	0.054	0.040	0.026	0.012	0.006	0.0	0.0	0.0	0.0	0.0	0.0	0.0	0.0	0.0
1300-1340	0.137	0.165	0.115	0.079	0.062	0.039	0.021	0.018	0.003	0.0	0.0	0.0	0.0	0.0	0.0
1340-1380	0.295	0.212	0.159	0.135	0.101	0.074	0.060	0.046	0.033	0.016	0.004	0.0	0.0	0.0	0.0
1900-1940	0.132	0.138	0.096	0.072	0.048	0.037	0.030	0.024	0.011	0.004	0.004	0.005	0.0	0.0	0.0
1940-1980	0.140	0.107	0.069	0.055	0.041	0.037	0.024	0.016	0.006	0.006	0.0	0.0	0.0	0.0	0.0
1980-2020	0.080	0.097	0.058	0.052	0.028	0.011	0.013	0.005	0.004	0.002	0.0	0.0	0.0	0.0	0.0

Table 5. Values of $G(\bar{w}, T; p_r, T_r)$ for the band center region, in which p_r and T_r are set, respectively, at 275 mb and 225 K. The units are $G\,(W/m^2)$, $T\,(K)$, $\bar{w}\,(g/cm^2)$.

$\log_{10}\bar{w}$	Temperature (K)					
	200	210	220	230	240	250
-5.0	24.77	27.89	31.36	35.29	39.79	44.97
-4.8	24.51	27.60	31.05	34.95	39.41	44.56
-4.6	24.20	27.25	30.66	34.52	38.94	44.04
-4.4	23.80	26.82	30.18	33.99	38.35	43.40
-4.2	23.32	26.28	29.59	33.34	37.64	42.61
-4.0	22.73	25.63	28.88	32.55	36.77	41.65
-3.8	22.02	24.84	28.00	31.59	35.70	40.47
-3.6	21.17	23.89	26.95	30.43	34.42	39.06
-3.4	20.15	22.77	25.71	29.05	32.90	37.37
-3.2	18.96	21.45	24.25	27.44	31.12	35.40
-3.0	17.60	19.94	22.57	25.58	29.06	33.12
-2.8	16.08	18.24	20.69	23.49	26.75	30.55
-2.6	14.42	16.40	18.64	21.21	24.21	27.73
-2.4	12.68	14.45	16.47	18.79	21.51	24.71
-2.2	10.91	12.47	14.24	16.31	18.73	21.59
-2.0	9.17	10.50	12.04	13.83	15.95	18.45
-1.8	7.49	8.61	9.91	11.42	13.22	15.36
-1.6	5.92	6.82	7.88	9.12	10.60	12.38
-1.4	4.46	5.16	5.99	6.97	8.14	9.56
-1.2	3.15	3.67	4.28	5.01	5.90	6.98
-1.0	2.04	2.39	2.82	3.34	3.97	4.76
-0.8	1.17	1.39	1.67	2.01	2.44	2.98
-0.6	0.57	0.70	0.86	1.08	1.35	1.70
-0.4	0.23	0.30	0.39	0.52	0.68	0.91
-0.2	0.08	0.12	0.17	0.24	0.34	0.48
-0.0	0.03	0.05	0.08	0.12	0.18	0.26
0.2	0.01	0.03	0.04	0.06	0.10	0.14
0.4	0.01	0.01	0.02	0.03	0.05	0.08
0.6	0.00	0.01	0.01	0.02	0.02	0.04

Table 5. (Continued)

$\log_{10} \overline{w}$	Temperature (K)					
	260	270	280	290	300	310
-5.0	50.99	58.01	66.19	75.70	86.73	99.46
-4.8	50.54	57.51	65.63	75.09	86.05	98.71
-4.6	49.97	56.88	64.94	74.32	85.20	97.76
-4.4	49.26	56.10	64.07	73.36	84.14	96.58
-4.2	48.39	55.14	63.01	72.18	82.82	95.12
-4.0	47.33	53.96	61.70	70.72	81.20	93.31
-3.8	46.03	52.52	60.11	68.95	79.23	91.11
-3.6	44.47	50.79	58.18	66.81	76.84	88.45
-3.4	42.60	48.72	55.88	64.25	73.99	85.25
-3.2	40.41	46.29	53.18	61.23	70.61	81.48
-3.0	37.88	43.48	50.04	57.73	66.69	77.08
-2.8	35.02	40.29	46.48	53.74	62.22	72.05
-2.6	31.88	36.77	42.53	49.30	57.22	66.42
-2.4	28.50	32.98	38.27	44.49	51.78	60.26
-2.2	24.99	29.01	33.78	39.41	46.00	53.69
-2.0	21.43	24.98	29.20	34.17	40.02	46.85
-1.8	17.91	20.97	24.60	28.90	33.97	39.89
-1.6	14.50	17.05	20.09	23.71	27.97	32.97
-1.4	11.26	13.32	15.78	18.72	22.19	26.27
-1.2	8.30	9.89	11.81	14.10	16.83	20.05
-1.0	5.72	6.90	8.34	10.06	12.13	14.57
-0.8	3.65	4.49	5.52	6.76	8.26	10.04
-0.6	2.15	2.72	3.42	4.29	5.34	6.60
-0.4	1.20	1.57	2.03	2.61	3.32	4.18
-0.2	0.66	0.89	1.19	1.57	2.03	2.59
-0.0	0.37	0.51	0.70	0.93	1.22	1.58
0.2	0.21	0.29	0.40	0.54	0.71	0.92
0.4	0.11	0.16	0.22	0.29	0.39	0.50
0.6	0.05	0.08	0.11	0.15	0.19	0.25

Table 6. Values of $G(\overline{w}, T; p_r, T_r)$ for the band wing region, in which p_r and T_r are set, respectively, at 550 mb and 256 K. The units are $G(W/m^2)$, $T(K)$, $\overline{w}(g/cm^2)$.

$\log_{10}\overline{w}$	Temperature (K)					
	200	210	220	230	240	250
-4.4	33.13	39.48	46.51	54.27	62.80	72.16
-4.2	32.99	39.31	46.32	54.06	62.56	71.90
-4.0	32.80	39.10	46.07	53.77	62.24	71.54
-3.8	32.55	38.81	45.75	53.40	61.82	71.07
-3.6	32.24	38.45	45.33	52.93	61.29	70.47
-3.4	31.85	37.99	44.80	52.33	60.61	69.71
-3.2	31.36	37.43	44.15	51.58	59.77	68.76
-3.0	30.77	36.74	43.36	50.67	58.74	67.60
-2.8	30.06	35.90	42.39	49.57	57.49	66.20
-2.6	29.21	34.91	41.25	48.27	56.01	64.52
-2.4	28.22	33.76	39.91	46.73	54.26	62.56
-2.2	27.09	32.43	38.37	44.97	52.25	60.29
-2.0	25.80	30.92	36.62	42.95	49.95	57.68
-1.8	24.35	29.21	34.64	40.67	47.35	54.73
-1.6	22.72	27.29	32.40	38.09	44.40	51.38
-1.4	20.90	25.14	29.89	35.18	41.07	47.59
-1.2	18.87	22.74	27.08	31.94	37.34	43.34
-1.0	16.67	20.13	24.02	28.38	33.26	38.68
-0.8	14.33	17.35	20.76	24.60	28.90	33.69
-0.6	11.94	14.51	17.41	20.69	24.39	28.52
-0.4	9.59	11.69	14.09	16.82	19.90	23.36
-0.2	7.38	9.04	10.95	13.14	15.62	18.44
0.0	5.41	6.67	8.14	9.83	11.76	13.97
0.2	3.76	4.68	5.76	7.01	8.47	10.14
0.4	2.47	3.10	3.86	4.76	5.81	7.04
0.6	1.51	1.93	2.44	3.06	3.80	4.67
0.8	0.87	1.13	1.47	1.88	2.38	2.97
1.0	0.47	0.63	0.85	1.11	1.44	1.85
1.2	0.25	0.35	0.48	0.65	0.87	1.14
1.4	0.13	0.20	0.28	0.39	0.53	0.71

Table 6. (Continued)

$\log_{10} \overline{w}$	Temperature (K)					
	260	270	280	290	300	310
-4.4	82.41	93.60	105.80	119.08	133.50	149.14
-4.2	82.11	93.27	105.44	118.69	133.08	148.67
-4.0	81.71	92.83	104.96	118.16	132.50	148.04
-3.8	81.19	92.26	104.32	117.46	131.74	147.22
-3.6	80.52	91.51	103.50	116.56	130.75	146.14
-3.4	79.67	90.57	102.47	115.42	129.50	144.78
-3.2	78.62	89.40	101.17	113.99	127.94	143.07
-3.0	77.32	87.96	99.58	112.24	126.01	140.96
-2.8	75.75	86.21	97.64	110.10	123.66	138.39
-2.6	73.88	84.12	95.32	107.55	120.85	135.31
-2.4	71.67	81.66	92.60	104.53	117.53	131.66
-2.2	69.12	78.81	89.43	101.02	113.66	127.41
-2.0	66.19	75.54	85.78	96.98	109.19	122.49
-1.8	62.86	71.81	81.62	92.35	104.07	116.84
-1.6	59.08	67.56	76.87	87.07	98.22	110.38
-1.4	54.79	62.74	71.48	81.07	91.56	103.01
-1.2	49.99	57.33	65.42	74.30	84.04	94.68
-1.0	44.70	51.37	58.72	66.82	75.71	85.45
-0.8	39.03	44.96	51.52	58.76	66.73	75.46
-0.6	33.15	38.30	44.01	50.34	57.32	64.99
-0.4	27.26	31.61	36.46	41.86	47.82	54.40
-0.2	21.62	25.19	29.20	33.66	38.63	44.12
0.0	16.49	19.33	22.54	26.14	30.15	34.61
0.2	12.07	14.20	16.75	19.57	22.72	26.24
0.4	8.46	10.10	11.98	14.11	16.52	19.22
0.6	5.69	6.88	8.25	9.82	11.61	13.63
0.8	3.69	4.53	5.51	6.64	7.94	9.41
1.0	2.34	2.92	3.60	4.39	5.31	6.35
1.2	1.47	1.86	2.33	2.87	3.50	4.21
1.4	0.92	1.18	1.49	1.85	2.27	2.75

Table 7. Upward fluxes at the top of the atmosphere, $F\uparrow(0)$, and downward fluxes at the earth's surface, $F\downarrow(p_s)$, in W/m^2. Percentage errors in fluxes are given in the parenthesis.

	Tropical		Sub-arctic winter	
	$F\uparrow(0)$	$F\downarrow(p_s)$	$F\uparrow(0)$	$F\downarrow(p_s)$
Exact	133.40	211.88	106.85	99.45
Present method	135.42 (+1.5%)	213.33 (+0.7%)	108.09 (+1.2%)	100.39 (+1.0%)
Rodgers-Walshaw method	132.44 (−0.7%)	215.97 (+1.9%)	106.61 (−0.2%)	100.38 (+1.0%)

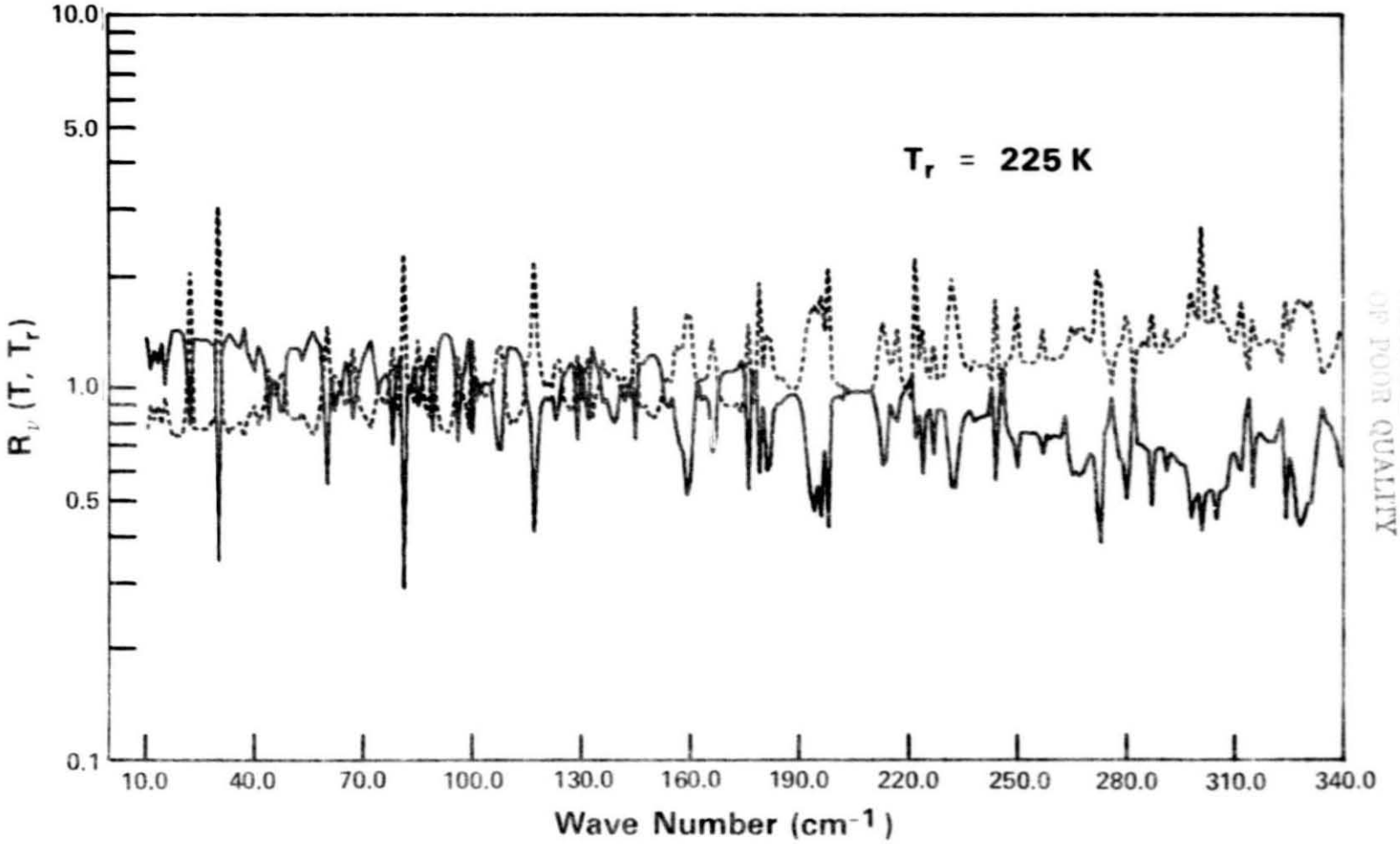

Figure 1a. Effect of temperature on the absorption coefficient, R_ν (T, T_r), in the band center region with T_r = 225 K. The dashed curve is for T = T_r + 40 K, and the solid curve is for T = T_r - 40 K.

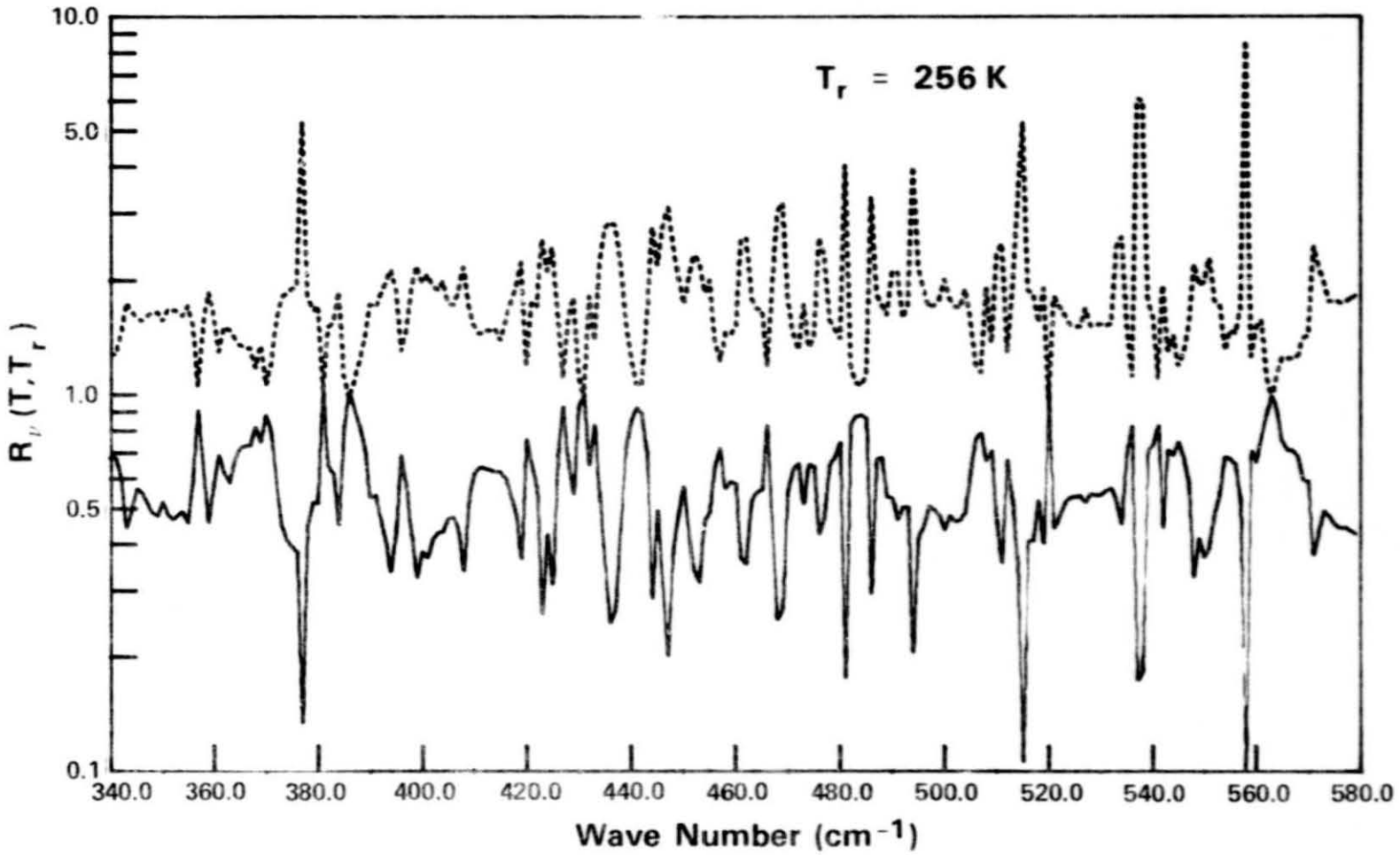

Figure 1b. Effect of temperature on the absorption coefficient, R_ν (T, T_r), in the band wing region with T_r = 256 K. The dashed curve is for T = T_r + 40 K, and the solid curve is for T = T_r – 40 K.

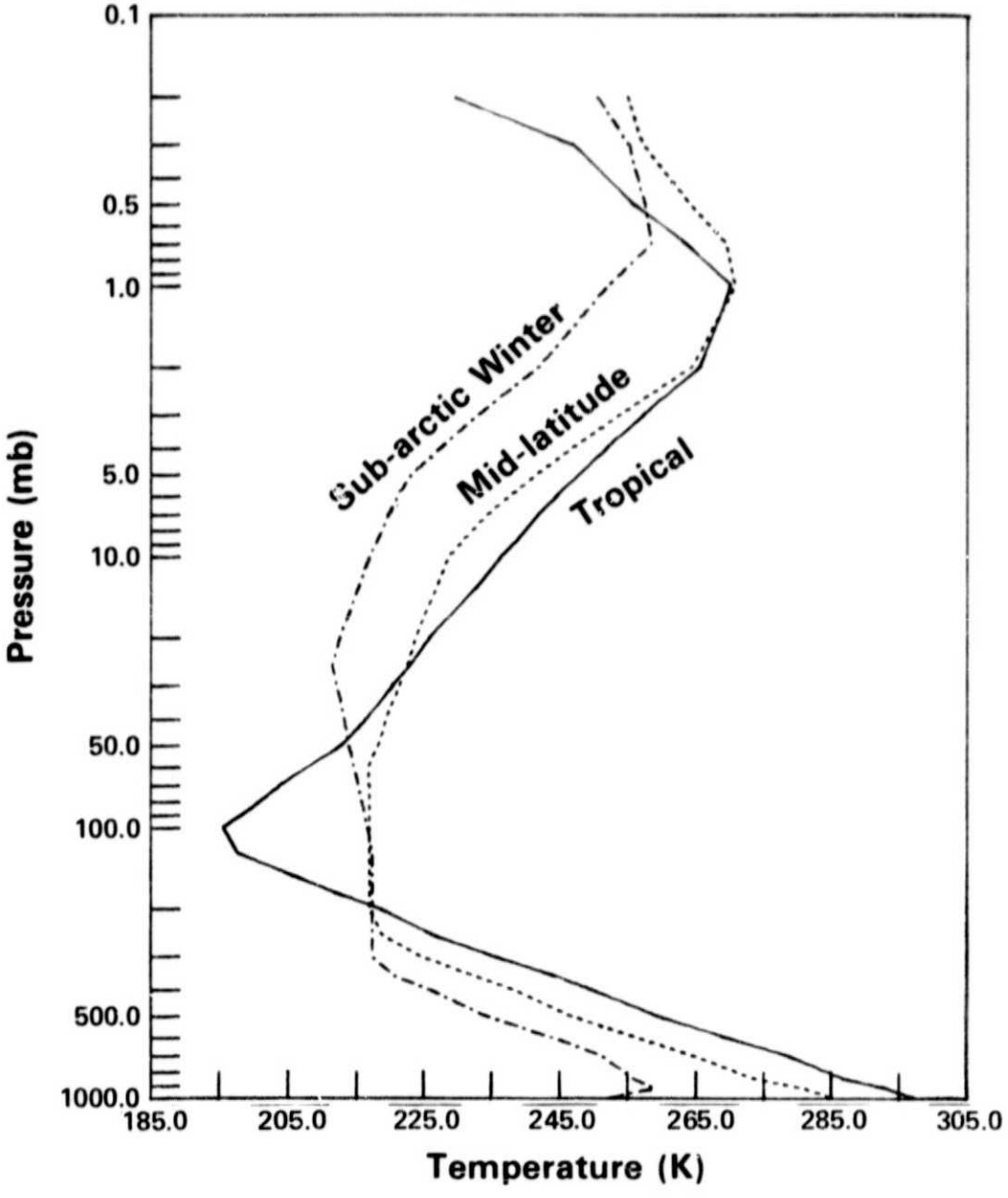

Figure 2a. Temperature profiles used in this study. The tropical and subarctic-winter profiles are from McClatchey et al. (1972)

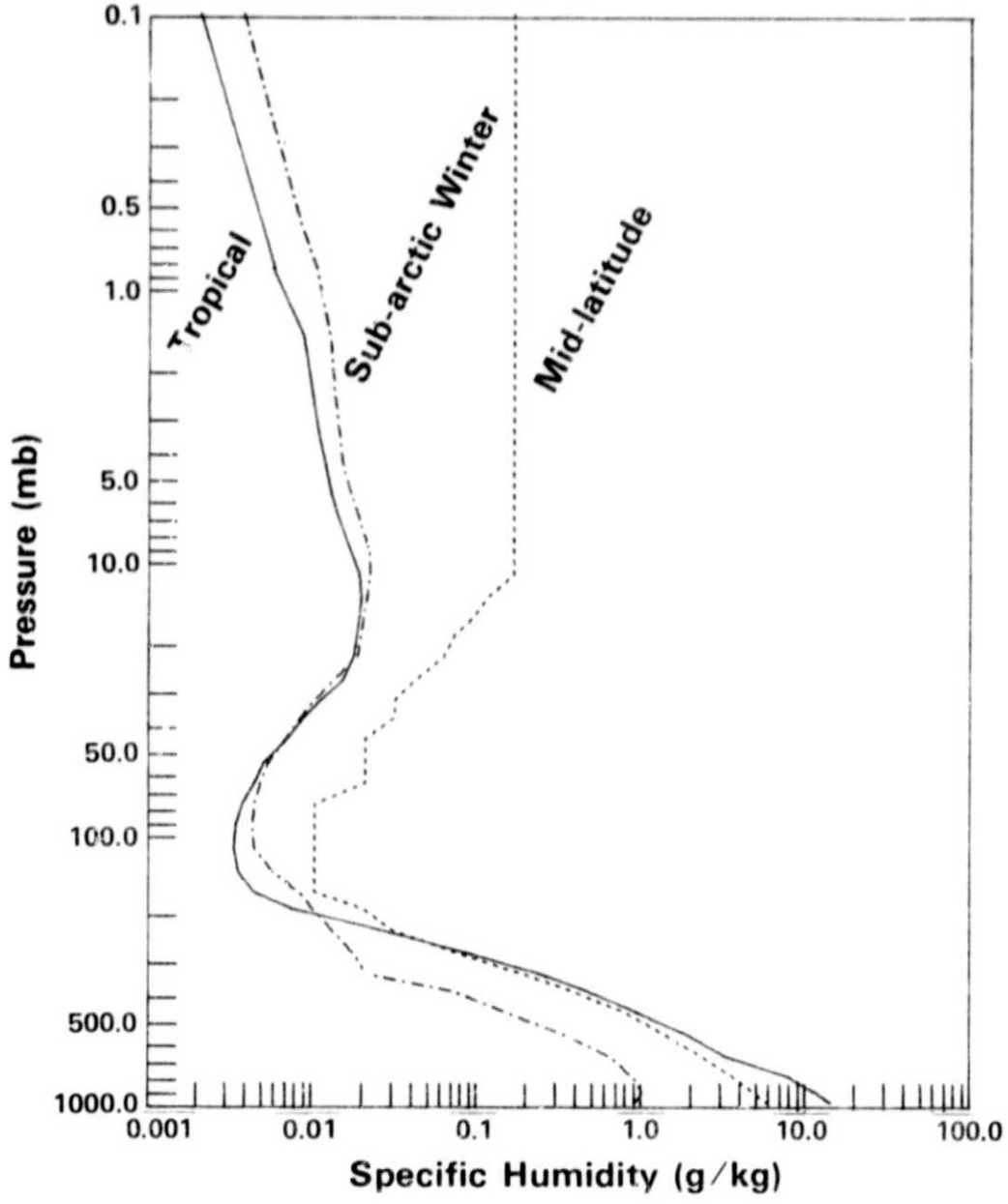

Figure 2b. Humidity profiles associated with the temperature profiles in Figure 2a.

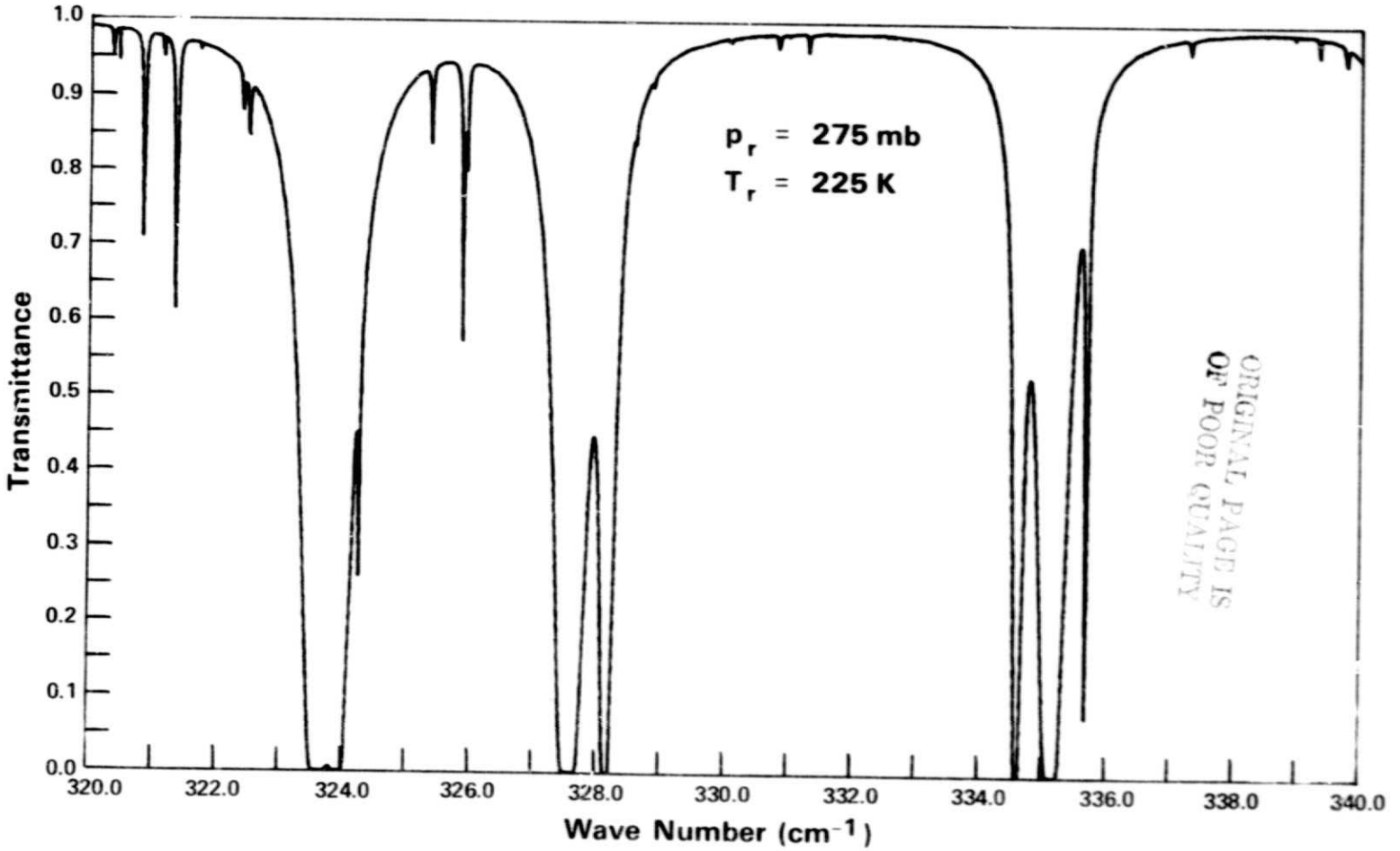

Figure 3a. Intensity transmittances between the 100- and 250-mb levels for the spectral region 320–340 cm^{-1}. A typical mid-latitude atmosphere was used for the computations. The solid curve was computed using the exact line-by-line method, and the dashed curve was computed using the far-wing approximation.

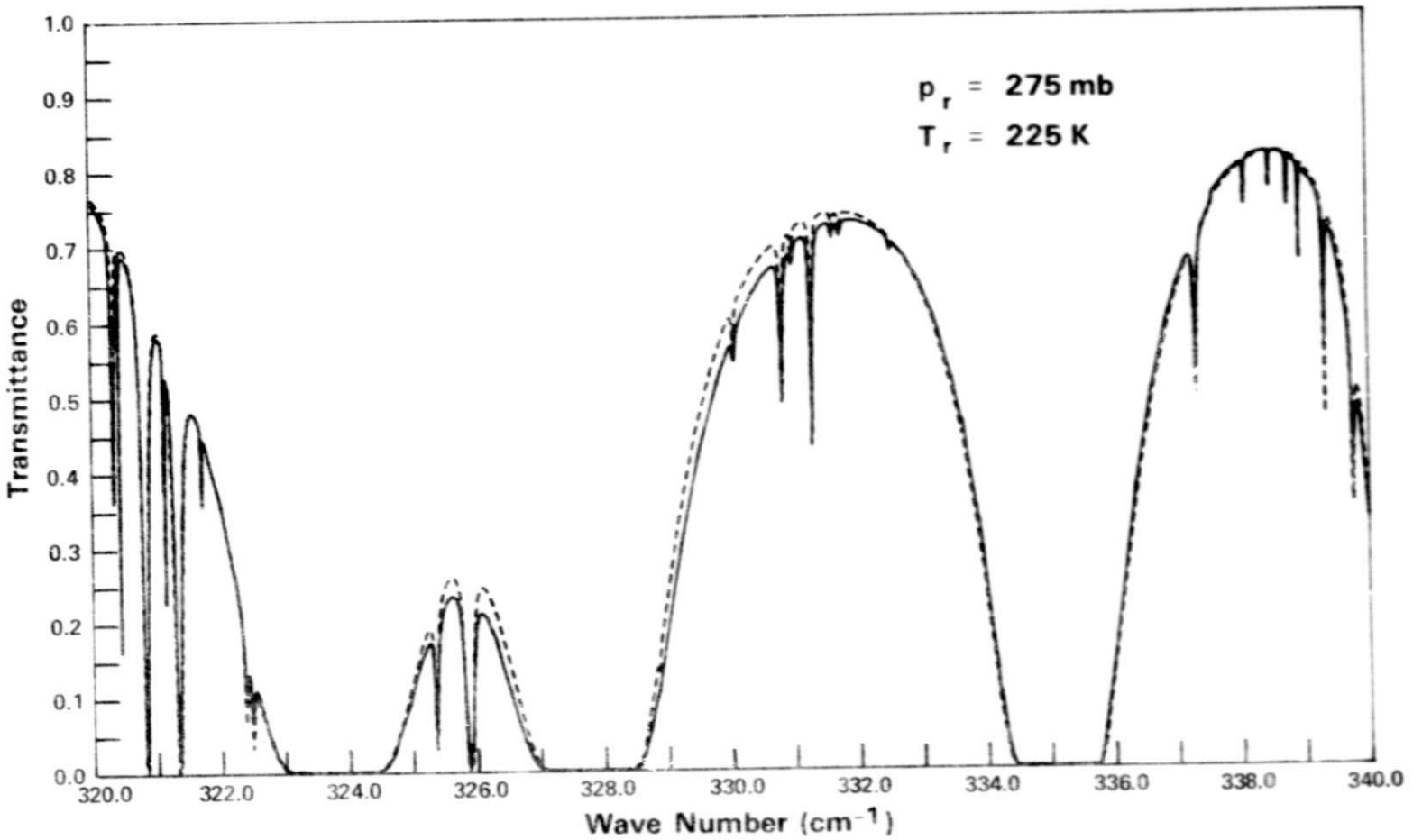

Figure 3b. Intensity transmittances between the 250- and 400-mb levels for the spectral region 320–340 cm^{-1}. A typical mid-latitude atmosphere was used for the computations. The solid curve was computed using the exact line-by-line method, and the dashed curve was computed using the far-wing approximation.

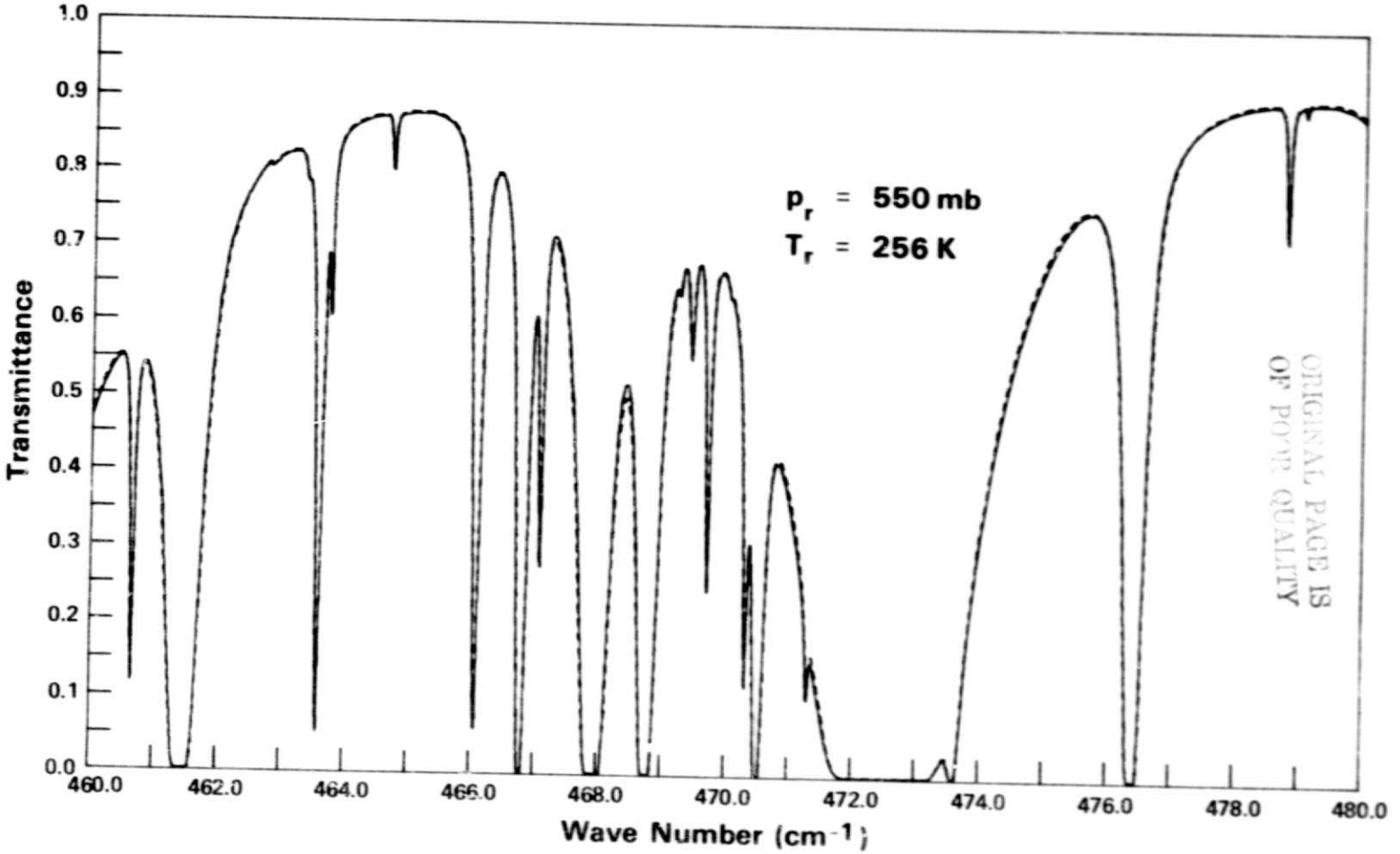

Figure 4. Intensity transmittances between the 300- and 600-mb levels for the spectral region 460–480 cm^{-1}. A typical mid-latitude atmosphere was used for the computations. The solid curve was computed using the exact line-by-line method, and the dashed curve was computed using the far-wing approximation.

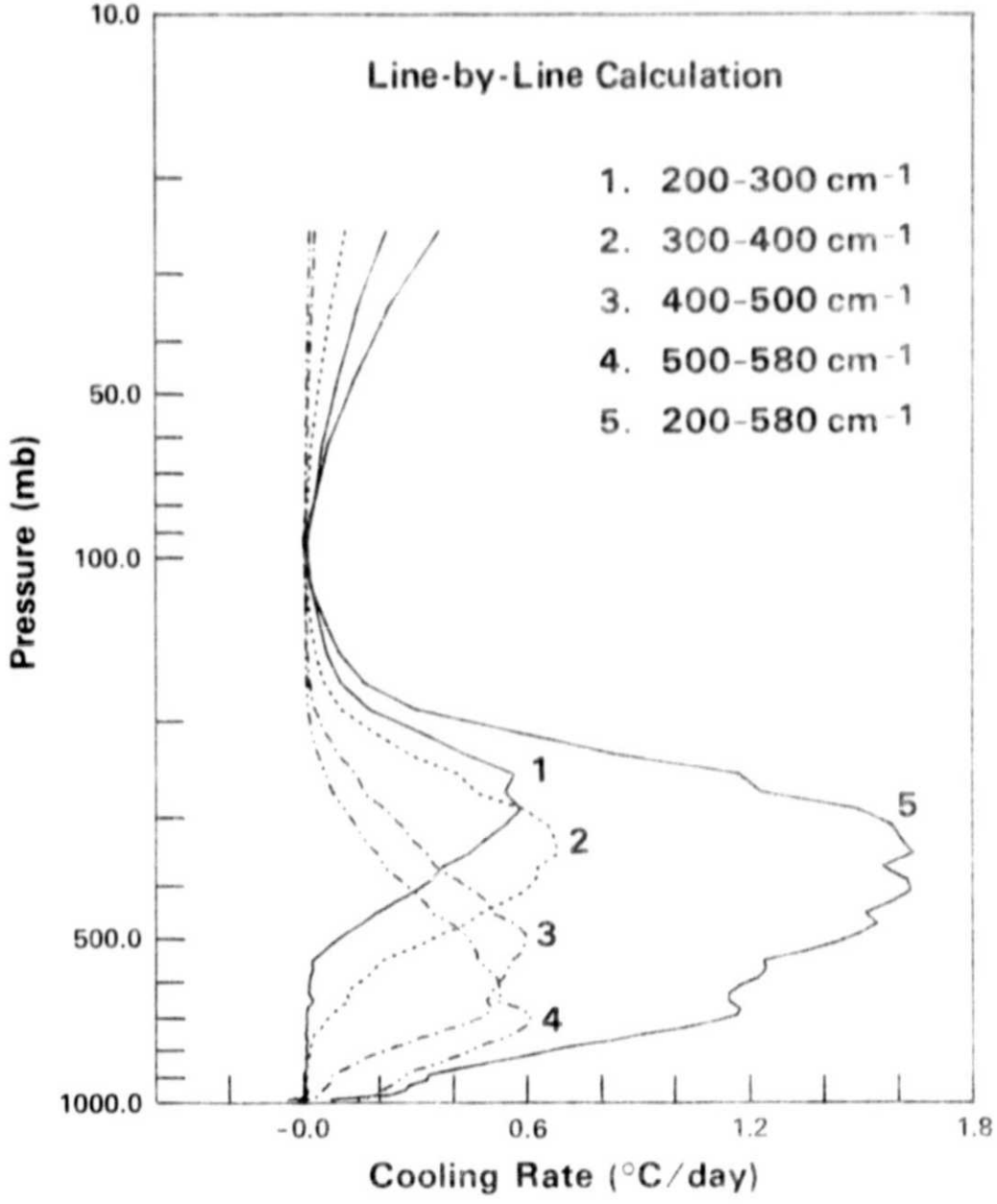

Figure 5a. Cooling rates computed from the exact line-by-line method in the spectral region 200–580 cm^{-1}. The clear tropical atmosphere shown in Figure 2 was used for the computations.

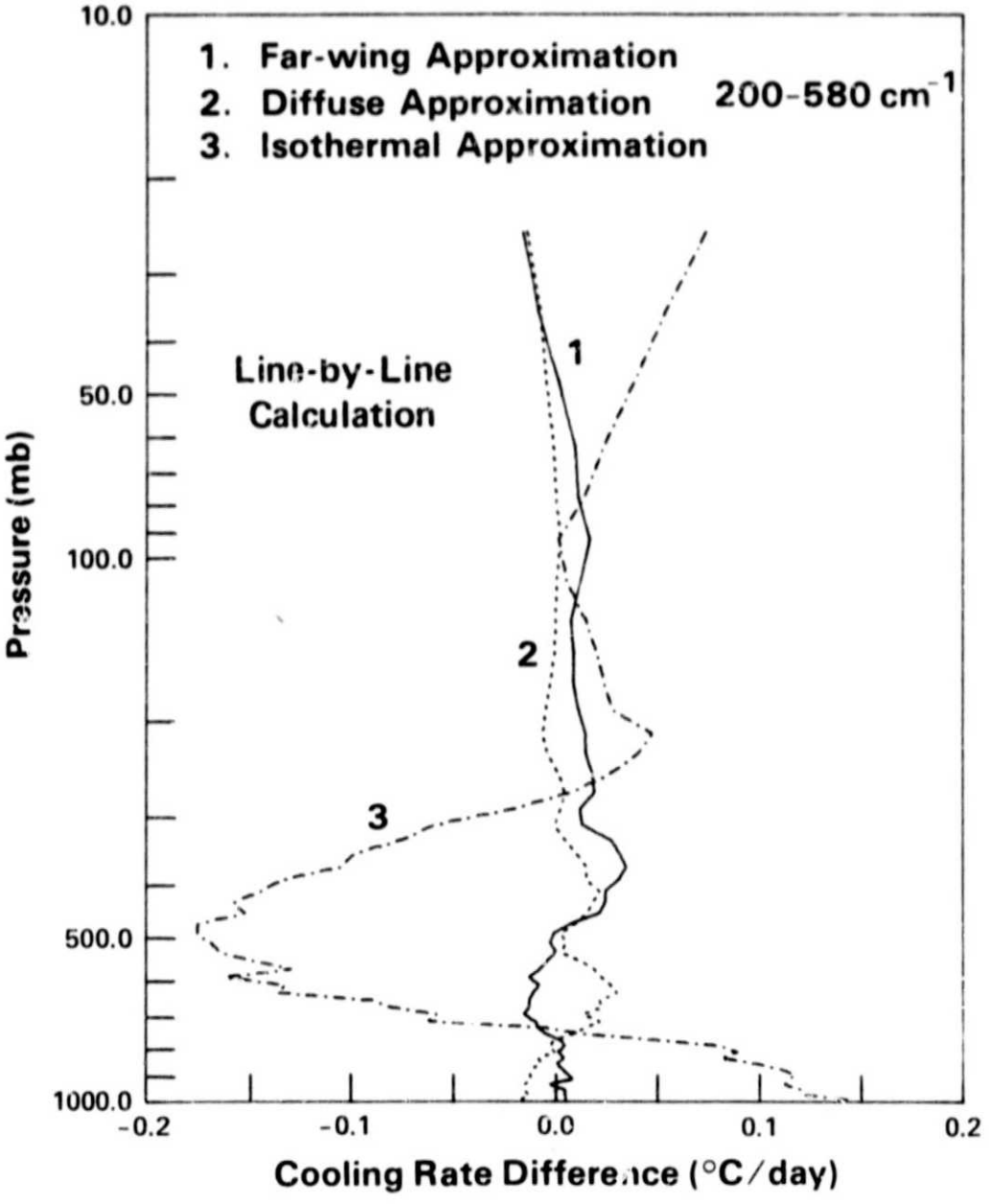

Figure 5b. Differences between the exact cooling rate and the cooling rates computed by using, respectively, the far-wing, the diffusivity, and the isothermal approximations for the spectral region 200–580 cm^{-1}.

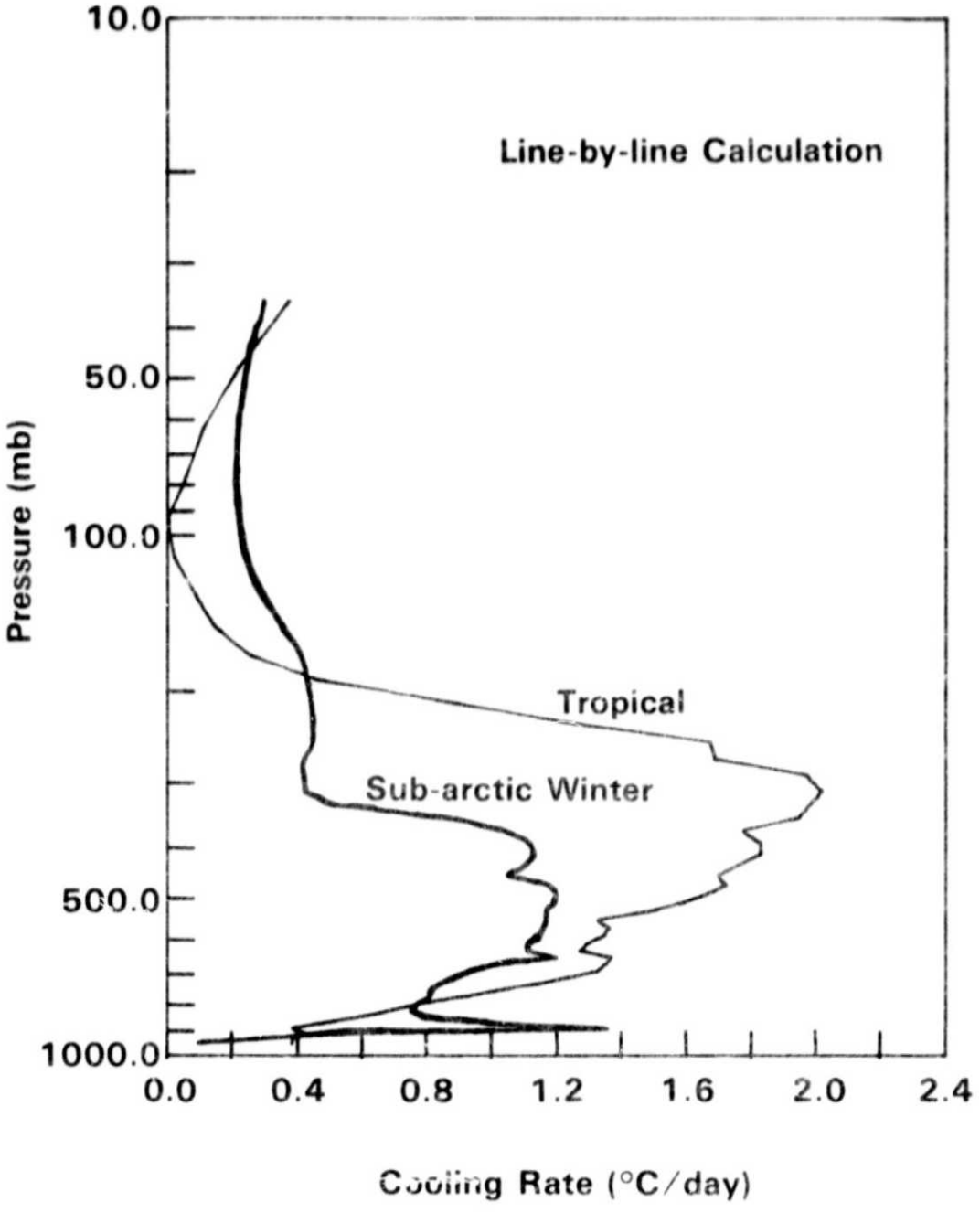

Figure 6a. Exact cooling rates in the 0–580 cm^{-1} and 1220–2020 cm^{-1} spectral regions for the clear tropical and subarctic-winter atmospheres shown in Figure 2.

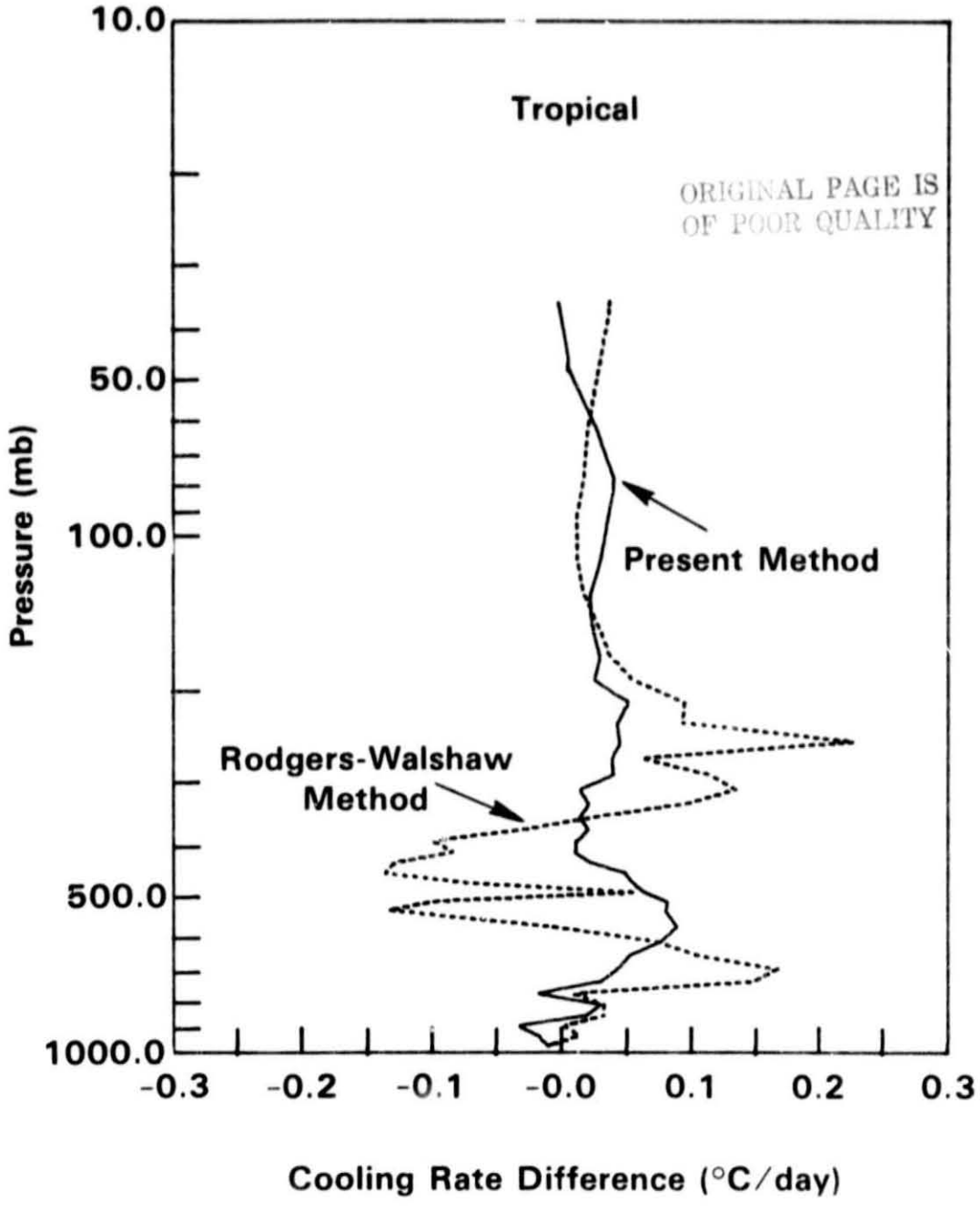

Figure 6b. Differences between the exact cooling rate and the cooling rates computed by using, respectively, the present method and the Rodgers-Walshaw method in the 0–580 cm^{-1} and 1220–2020 cm^{-1} regions for the clear tropical atmosphere shown in Figure 2.

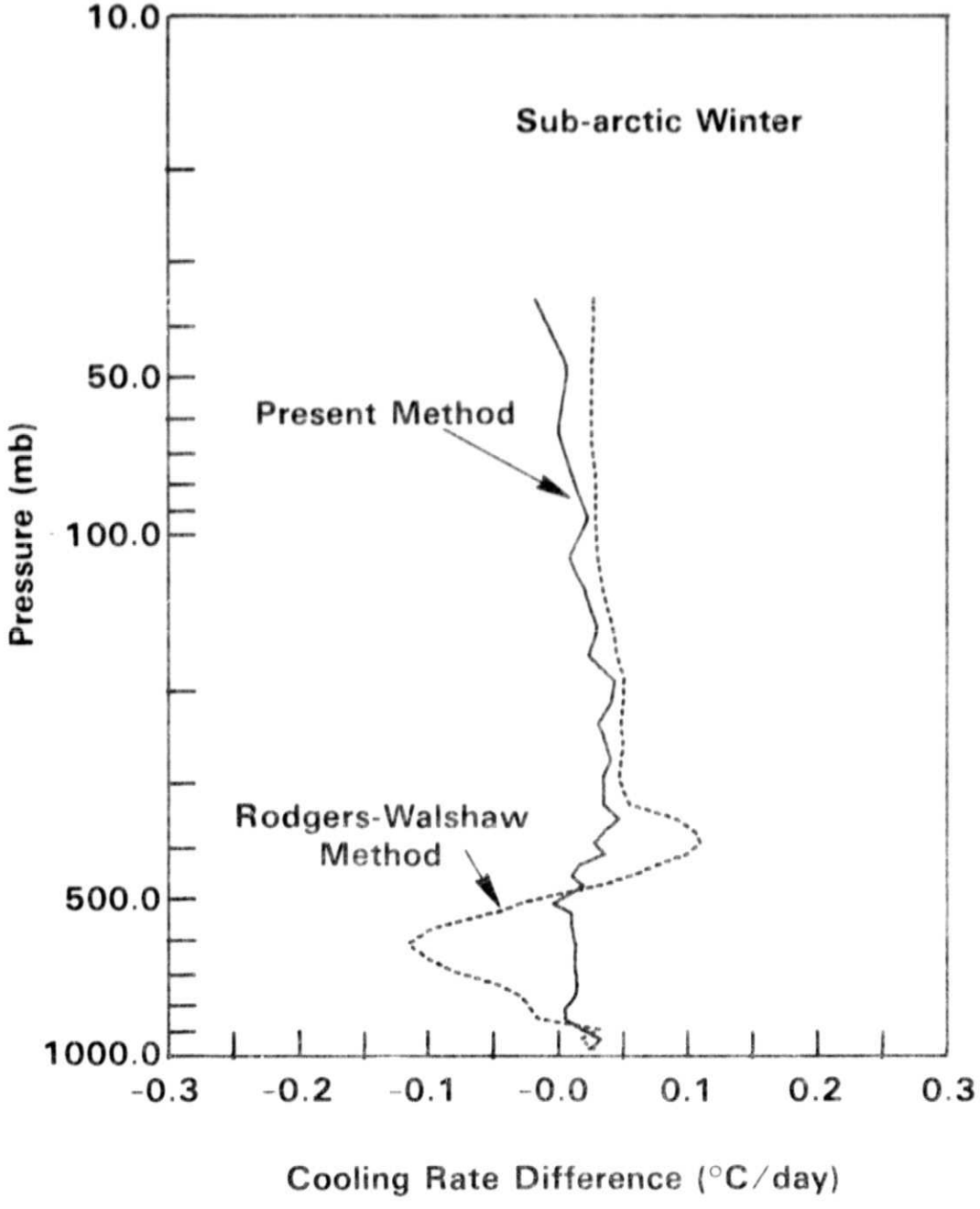

Figure 6c. Differences between the exact cooling rate and the cooling rates computed by using, respectively, the present method and the Rodgers-Walshaw method in the 0–580 cm^{-1} and 1220–2020 cm^{-1} regions for the subarctic-winter atmosphere shown in Figure 2.